Carrier dynamics and excitation of Eu^{3+} ions in GaN

Dolf Timmerman,[1] Brandon Mitchell,[2] Shuhei Ichikawa,[1] Masaya Nagai,[3] Masaaki Ashida,[3] and Yasufumi Fujiwara[1]

[1]*Graduate School of Engineering, Osaka University, 2-1 Yamadaoka, Suita, Osaka 565-0871, Japan*

[2]*Department of Physics and Engineering, West Chester University, West Chester, Pennsylvania 19383, USA*

[3]*Graduate School of Engineering Science, Osaka University, 1-3 Machikaneyama, Toyonaka, Osaka 560-8531, Japan*

(Received 26 March 2020; revised manuscript received 31 May 2020; accepted 2 June 2020; published 17 June 2020)

The carrier mobility and dynamics of nonequilibrium carriers in Eu-doped GaN have been determined by above-band-gap, optically excited, time-resolved terahertz spectroscopy and compared with that of undoped GaN. The carrier mobility of GaN:Eu was an order of magnitude smaller than that of a similarly grown undoped GaN layer. Two time constants were observed in the carrier relaxation dynamics for GaN:Eu. A fast one (2.2 ps), which we related to an efficient nonradiative carrier trap, and a slower one (∼85 ps) related to Eu-related traps. Ultrafast photoluminescence spectroscopy shows that Eu-related emission is observed within 100 ps after a pulsed excitation. These values set an upper value to the energy-transfer time from the Eu-related trap to Eu^{3+} ion and underlie the high efficiency of the excitation of Eu^{3+} ions in GaN.

DOI: 10.1103/PhysRevB.101.245306

Eu-doped GaN shows great promise for its application as a red-light emitter with temperature-insensitive, sharp, and stable emission based on the well-developed GaN platform. Current injection is relatively easy in these materials, and high optical output powers of device structures have been shown [1,2]. When the GaN host is optically excited, free carriers are generated which can subsequently transfer their energy to incorporated Eu^{3+} ions. Typically, the energy transfer from the carriers takes place via an intermediate state, generally described as a Eu-related trap [3–5]. Recently, we have shown that for similar GaN:Eu layers grown on a GaN substrate, the external quantum efficiency of photoluminescence can reach 29% at room temperature under pulsed excitation conditions [6]. It was found that the main limitation in the energy transfer from host to Eu^{3+} ions originates from an efficient competing trapping center at low pump fluences (nonequilibrium carrier density $\Delta N < 5 \times 10^{17}\,\mathrm{cm}^{-3}$), while at high pump fluences the efficiency is limited by the concentration of high-efficiency Eu^{3+} sites ($\Delta N > 5 \times 10^{19}\,\mathrm{cm}^{-3}$). In this work we determine the dynamics of the nonequilibrium carriers in GaN:Eu and show how they are primarily determined by the presence of Eu^{3+} ions, and high-efficiency nonradiative traps at intermediate pump fluences. The small mobility and short carrier lifetime has an additional advantage of lowering carrier diffusion lengths. This is especially beneficial for micro-LED applications in high-resolution displays, as sidewall-related recombination strongly limits device efficiencies when going to smaller feature sizes [7,8]. The timescale related to the trapping of carriers to the Eu-related traps naturally sets a lower limit for the energy-transfer time from the host to the Eu^{3+} ions. Additional time-resolved photoluminescence (PL) measurements confirm that the Eu^{3+} ions are excited on the same ultrafast timescale as the carrier trapping takes place. These results show that the energy from the carrier trap to the Eu^{3+} ion is very fast and underpins the high PL quantum efficiency (QE) of these materials.

The ultrafast carrier dynamics were determined by the time-resolved terahertz spectroscopy (TRTS) technique. The TRTS measurement system [9] was based on a 1-kHz amplified Ti:sapphire laser with a duration of 35 fs and a center wavelength of 800 nm (Spitfire, Spectra-Physics). The output beam was divided into three paths using two beam-splitters for optical excitation, terahertz pulse generation, and detection. The beam for optical excitation was guided through an optical parametric amplifier (TOPAS, Spectra-Physics) to generate a wavelength of 355 nm, with a maximum fluence of 24 $\mu\mathrm{J/cm}^2$ on the sample, which could be lowered by optical density filters. Terahertz pulses from two-color (ω and 2ω) excited air plasma were focused on the sample with p polarization at a 30° incidence angle. The reflected terahertz pulse was detected with an electro-optic sampling method by using a 300–μm-thick (110)-oriented GaP crystal. The time profile of the terahertz pulses was obtained by varying the time delay, t, between the terahertz and sampling pulses. Terahertz pulses reflected on an Al plane mirror were used as a reference to evaluate the absolute reflectivity precisely. For the optical excitation, unfocused pulses at normal incidence were used. The transient reflection response was obtained by varying the pump-probe delay, Δt_p.

Additionally, induced absorption (IA) experiments were performed by a Yb:KGW laser (Pharos PH1-10W, Light Conversion, Vilnius, Lithuania) operating at 50 kHz with a ∼200 fs pulse width and ∼0.2 mJ pulse energy at an output wavelength of 1030 nm, which was used to pump an optical parametric amplifier, Orpheus-HP (Light Conversion, Vilnius, Lithuania), in order to generate excitation pulses with a wavelength of 350 nm. These were guided via a delay stage and incident on the sample under 15° (spot diameter 1 mm, fluence 7 $\mu\mathrm{W/cm}^2$). A white-light-continuum probe beam was generated by focusing a small part of the output of the Pharos through a yttrium aluminum garnet (YAG) crystal. The probe pulse was

detected after passing the sample by a Thorlabs CCM200/m spectrometer.

For the time-resolved PL the same laser was employed operating at 1 kHz with a wavelength of 350 nm. The excitation laser was guided through a circular pinhole in order to obtain a homogenous intensity throughout the excitation spot (top-hat profile). Luminescence was spectrally dispersed by a SpectraPro 300i spectrometer (Acton Research Corporation) and detected with a streak camera (Hamamatsu C4334) for a 10/1-ns time window with a resolution of 150/15 ps.

The samples in this work were grown by organometallic vapor-phase epitaxy (OMVPE) on GaN and sapphire substrates, where trimethylgallium (TMGa) and ammonia (NH_3) were used as the gallium and nitrogen sources, respectively. The reactor pressure was maintained at 100 kPa during growth. For the GaN:Eu layers, bis(normal-propyltetramethylcyclopentadienyl)europium ($EuCp^{pm}{}_2$) was used as the Eu source. The Eu source and transfer lines were maintained at 125 °C and 135 °C, respectively. The Eu concentration was approximately $1.0 \times 10^{20}\,\mathrm{cm}^{-3}$ as determined from secondary ion mass spectroscopy. The growth temperature of the optical active layer was 960 °C, which is the optimal growth temperature for GaN:Eu [10,11]. Two sets of GaN and GaN:Eu layers were grown, on GaN and sapphire substrate, respectively. The GaN substrate was used in the IA experiments because it prevents the appearance of interference effects which arise due to differences in the refractive index between the optical active layer and substrate. In prior experiments, this turned out to be too detrimental to allow for a proper interpretation of data. The sapphire substrates where used in the TRTS experiments, as the *n*-doped GaN substrate induced a strong terahertz reflectance signal.

Firstly, the charge carrier conductivity and mobility of the layers was determined by optically excited TRTS. The photoconductivity is probed by the broadband terahertz pulse at *p* polarization at a 30° incidence angle in reflection mode. Figure S1 in the Supplementary Material [12] shows the time profiles of the reflected terahertz pulse on the sample $E_0(t)$ and its change under the photoexcitation $\Delta E(t)$. The field amplitude of the terahertz pulse increases with the photoexcitation. This change originates from the photoexcited carriers near the sample's surface. Assuming a *p*-polarized terahertz pulse incidence with an incident angle of θ_1, the sheet conductivity σ_s of the photoexcited carriers can be expressed as a function of $\Delta E/E_0$,

$$\sigma_s \approx \frac{1}{Z_0 \cos\theta_1} \frac{2r_0}{(r_0-1)^2} \Delta E/E_0.$$

Here, Z_0 is the impedance in vacuum, and $r_0 = 0.46$ is the reflectance of the sample with the refractive index of the sample $n_2 = 3.06$ [13]. This formula is derived from the conventional Maxwell's boundary condition, as shown in the Supplementary Material. This is inherently available for the Fourier-transformed $\Delta E/E_0$, but we evaluated the sheet conductivity from the peak of E_0 and ΔE in time domain. This procedure can be applied when $\Delta E/E_0$ is evaluated experimentally in the low-frequency limit. This is supported by the similar phase of $E_0(t)$ and $\Delta E(t)$ in Fig. S1, implying a real value of the conductivity characteristic of the conventional Drude model in the low-frequency limit

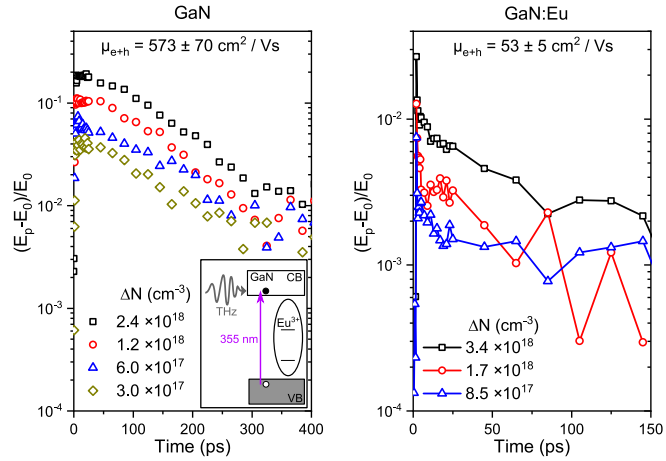

FIG. 1. Differential reflectivity of the terahertz peak electric field as a function of pump-probe delay time for various induced nonequilibrium carrier densities. The inset shows a schematic of the experiment.

[14]. The differential reflectivity of the terahertz peak electric fields as a function of pump-probe delay time for various induced nonequilibrium carrier densities are shown in Fig. 1 for both layers (N.B. all nonequilibrium carrier densities are below the Mott density, $\sim 10^{19}\,\mathrm{cm}^{-3}$ at room temperature [15,16]). These are used to determine the time evolution of the average photoconductivity, which is proportional to the carrier concentration. The excitation photon energy of 3.49 eV (355 nm) is only about 60 meV above the GaN band gap, and typical carrier cooling time of nonequilibrium carriers is very fast in GaN at the used carrier concentrations (~200 fs [17]), i.e., much faster than the time resolution of the system. The doping of Eu^{3+} ions at the used concentration is not expected to have a considerable effect on this, so we can exclude any carrier-cooling-related effects to be observed in this experiment. The real part of the conductivity is related to the direct current conductivity in the low-frequency limit by $\sigma = eN\mu$, where e is the electron charge and N and μ are the charge carrier density and mobility, respectively. In bulk semiconductors photoexcitation leads generally to equal numbers of electrons and holes with unit quantum yield, so the conductivity is determined by the sum of the electron and hole contributions. The changes in conductivity following optical excitation are sampled directly in TRTS, giving a differential sheet conductivity of $\Delta\sigma_s = e\,\Delta N\,d(\mu_e + \mu_h)$, where $d = 100\,\mathrm{nm}$ is the thickness of the photoexcited layer, estimated by the inverse of the absorption coefficient. From the figure we can see that the value of the mobility of GaN:Eu is about an order of magnitude lower than the GaN layer. Next to the values of mobility, the free-carrier lifetimes are also considerably different. While the GaN layer shows a nearly single-exponential decay of ~150 ps for the different nonequilibrium carrier values, GaN:Eu shows a biexponential decay with a fast picosecond initial decay (the time resolution of the system) and a longer component of ~85 ps. We do note that in the case the of GaN:Eu, the short initial lifetime is similar to the terahertz pulse length (~1 ps). Furthermore, due to the 30° incidence of the terahertz pulse and the spot size of

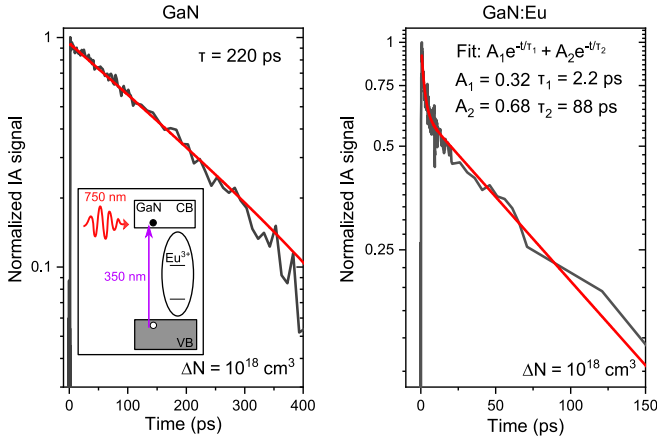

FIG. 2. Transient absorption signal for GaN and GaN:Eu grown on GaN substrate. The red line indicates a single-exponential fit (GaN) and a double exponential fit (GaN:Eu) of the data. The inset shows a schematic of the experiment.

2 mm, there is a time difference at both ends of the beam. These factors will lead to uncertainty in the evaluation of the mobility, and initial dynamics cannot be properly determined.

After establishing the free-carrier dynamics by TRTS, both layers were studied by transient IA spectroscopy after an excitation pulse of 350 nm. This experiment has a better time resolution than TRTS and is only limited by the duration of the optical pump and probe pulses. The normalized IA signal for both samples at a detection wavelength of 750 nm are depicted in Fig. 2. This wavelength was chosen as it is the longest probe wavelength with a good signal-to-noise ratio in the white light probe, while it should not be influenced by the near-band-edge response of GaN. Similarly as the TRTS results, GaN shows a single-exponential decay with a decay constant of 220 ps, while GaN:Eu shows a biexponential decay with an initial 2.2-ps time constant followed by one of 88 ps. Although the probing wavelength is much shorter than in the case of the TRTS experiment, the similarity in dynamics endorses that the IA signal is primarily determined by nonequilibrium carriers. The difference in carrier lifetime in GaN is a result of the substrate used, where the non-lattice-matched sapphire substrate produces a lower-crystal-quality GaN, which reduces the free-carrier lifetime. For GaN:Eu the dynamics are nearly identical, indicating that the incorporated Eu^{3+} ions almost fully determine them, independent of substrate. Additionally, since the time resolution is better for the transient IA, we use their dynamics to compensate the absolute value of the terahertz conductivity for short times, getting more reliable values of the conductivity for GaN:Eu. Following this methodology and the above formula for the combined electron and hole mobility, for the induced carrier concentrations in the figures we find combined mobility values of 573 ± 70 and $53 \pm 5\ cm^2/Vs$ for the GaN and GaN:Eu layer, respectively.

It is well known that there exist multiple incorporation sites of the Eu^{3+} ions in the GaN host. The majority center in GaN:Eu, which is referred to as OMVPE4 (Eu1), comprises about 90% of the total Eu^{3+} ions [3,5,18,19] and has a relatively small excitation cross section. The Eu sites that have a large excitation cross section are known as OMVPE7 (Eu2) and OMVPE8 (Eu2*), which have been shown to be different charge states for the same defect configuration [20]. For these Eu^{3+} ions, the excitation from the related trap takes place directly to the $^5D_0$ state [21,22]. Thus, following the emission from the $^5D_0$ state can give direct information about the time constant related to the energy transfer from the trap state to these Eu^{3+} ions. Figure 3(a) shows the initial PL decay around the main emission peak originating from the $^5D_0 \rightarrow {}^7F_2$ transition after an excitation pulse. There is a broad emission band over the whole spectral range which decays with a time constant of ∼3 ns and originates from native defects [23]. On top of this defect-related band, the emission originating from Eu^{3+} can be observed. Since the PL lifetime of Eu^{3+} is very long, the amount of luminescence in the nanosecond time window is extremely weak, an estimated 10^{12} Eu^{3+} ions cm^{-3} can undergo a radiative transition in

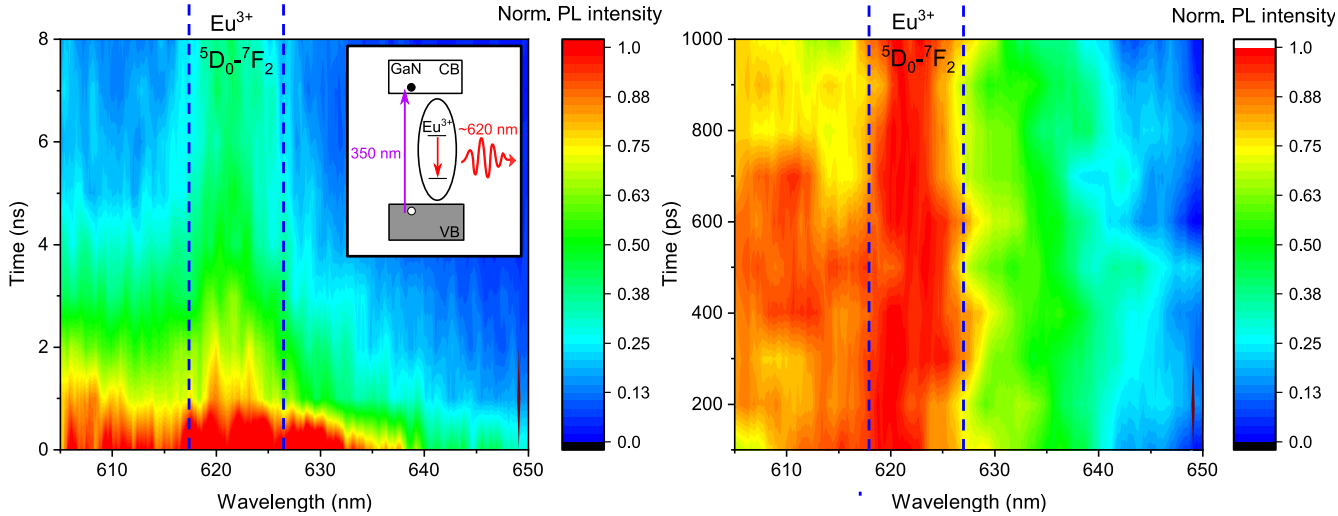

FIG. 3. Time-resolved photoluminescence spectrum around the $^5D_0$-$^7F_2$ transition of Eu^{3+}. Left: First 8 ns after a pulsed excitation. The inset shows a schematic of the experiment. Right: First nanosecond obtained by subtraction of the defect band and normalized to the maximum intensity for each time point.

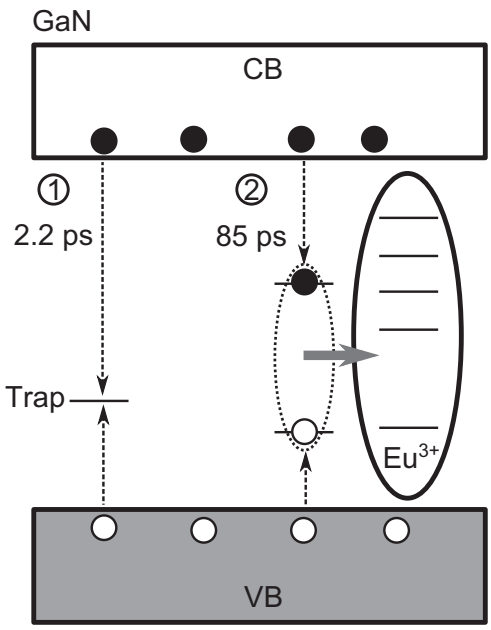

FIG. 4. Schematics of the two processes responsible for the carrier trapping and their associated times: (1) Ga-vacancy-related trap and (2) Eu-related trap. Gray arrow indicates the energy transfer from the Eu-related trap to the Eu^{3+} ion.

this time window, and the contribution of other defect-related radiative transitions, with typical concentrations of $10^{15}\,\mathrm{cm}^{-3}$ and much shorter lifetime [23–25], will dominate. In order to get information on the Eu^{3+} excitation in the 1-ns time window, the emission has been integrated in slices of 100 ps, and subsequently, the defect band has been subtracted by taking an average intensity at the long-wavelength side. The normalized emission intensity of this data treatment is given in Fig. 3(b). It can be seen that even in the first 100-ps slice the Eu^{3+} emission is already visible; however, a rise in dynamics cannot be determined.

The total recombination rate of excess carriers in a semiconductor is generally determined by Shockley-Read-Hall, radiative, and Auger recombination, with the total rate given by $R = R_{\mathrm{SRH}} + R_{\mathrm{rad}} + R_{\mathrm{Auger}} = A + Bn + Cn^2$, where A, B, and C, are the SRH, radiative and Auger coefficients, respectively. For GaN, typical values of the Auger coefficient C are on the order of $10^{-30}\,\mathrm{cm}^6/\mathrm{s}$ [26], which gives only a negligible contribution for the carrier densities used in this study. Furthermore, for bulk GaN, the fluence-dependent quantum efficiency of band-edge emission is typically $<1\%$ [27], which is also negligible. In short, the recombination rate is nearly fully determined by the SRH rate. In the SRH model, material impurities introduce deep energy levels within the band gap which act as recombination (or trap) centers [28]. The concentration of these defects and the efficiency with which they can trap determine their associated SRH rate. For a specific trap, the SRH rate is given by $R_{\mathrm{SRH}} = N_{\mathrm{T}} v_{\mathrm{T}} \sigma_{\mathrm{T}}$, where N_{T} is the trap concentration, v_{T} the mean thermal velocity of carriers, and σ_{T} the capture cross section. The mean thermal velocity of the carriers is given by $(3k_BT/m^*)^0$ [5], where k_B is the Boltzmann constant, T the temperature, and m^* the effective mass of the carrier. In Ref. [6] we showed that the PL quantum efficiency is limited by a highly efficient carrier trap with a carrier capture cross section of $\sim 10^{-13}\,\mathrm{cm}^2$ and a maximum trap concentration of $2 \times 10^{17}\,\mathrm{cm}^{-3}$, which is likely related to Ga vacancies. The absence of this fast component in the GaN epilayer is consistent with the notion that the incorporation of Eu^{3+} ions increases the concentration of Ga vacancies, which has also been concluded from positron-annihilation spectroscopy [10]. With these values we can expect an SRH time constant of ~ 2 ps, very close to the observed time constant of 2.2 ps. Also, the relative contribution of the fast component and the estimated carrier density are in line with these values. For the high-efficiency sites, an effective excitation cross section of $1.6 \times 10^{-15}\,\mathrm{cm}^2$ and estimated concentration of $\sim 10^{18}\,\mathrm{cm}^{-3}$ gives an SRH rate of ~ 50 ps, i.e., close to the observed 85 ps [6]. These results lead us to conclude that the fast component in the carrier dynamics is related to carrier trapping by the efficient trap and the slower component due to a Eu-related trap. A schematic model of these two pathways is shown in Fig. 4.

Finally, we comment on the energy transfer from the Eu-related trap state to the Eu^{3+} ions, indicated by the gray arrow in Fig. 4. From the PL results it is known that Eu-related emission is observed within 100 ps after excitation, and from the carrier dynamics a related trapping time of 85 ps was observed. Since the total energy-transfer time from host to Eu^{3+} ion is determined by the sum of the trapping time and the energy-transfer time, we conclude that the energy-transfer time has to be considerably faster than 100 ps. We note that a similar timescale has been concluded for the energy transfer in another rare-earth-doped semiconductor system: Er,O:GaAs [29].

We have investigated the ultrafast nonequilibrium carrier dynamics and PL properties of GaN:Eu. Two time constants were found in the carrier dynamics: a fast one of 2.2 ps, which has been associated to an efficient nonradiative carrier trap, likely related to Ga vacancies, and a slower one of 85 ps, which is due to capture of carriers by Eu-related traps. The PL dynamics show that Eu-related emission is observed within 100 ps after a pulsed excitation of the host material. These results demonstrate that the energy transfer from the Eu-related trap to Eu^{3+} ion must occur on a timescale considerably faster than 100 ps and is at the basis of the high PL QE that has been observed in this material. Additionally, the short carrier diffusion length due to low mobility and short free-carrier lifetime in this material can strongly limit sidewall-related nonradiative processes in micro-LED applications.

This work was partly supported by a Grant-in-Aid for Specially Promoted Research (Grant No. 18H05212) from the Japan Society for the Promotion of Science.

[1] W. Zhu, B. Mitchell, D. Timmerman, A. Koizumi, T. Gregorkiewicz, and Y. Fujiwara, MRS Adv. **2**, 159 (2017).

[2] B. Mitchell, V. Dierolf, T. Gregorkiewicz, and Y. Fujiwara, J. Appl. Phys. **123**, 160901 (2018).

[3] Z. Fleischman, C. Munasinghe, A. J. Steckl, A. Wakahara, J. Zavada, and V. Dierolf, Appl. Phys. B **97**, 607 (2009).
[4] N. Woodward, J. Poplawsky, B. Mitchell, A. Nishikawa, Y. Fujiwara, and V. Dierolf, Appl. Phys. Lett. **98**, 011102 (2011).
[5] Y. Fujiwara and V. Dierolf, Jpn. J. Appl. Phys. **53**, 05FA13 (2014).
[6] D. Timmerman, B. Mitchell, S. Ichikawa, J. Tatebayashi, M. Ashida, and Y. Fujiwara, Phys. Rev. Appl. **13**, 014044 (2020).
[7] J.-T. Oh, S.-Y. Lee, Y.-T. Moon, J. H. Moon, S. Park, K. Y. Hong, K. Y. Song, C. Oh, J.-I. Shim, H.-H. Jeong, J.-O. Song, H. Amano, and T.-Y. Seong, Opt. Express **26**, 11194 (2018).
[8] P. Tian, J. J. D. McKendry, Z. Gong, B. Guilhabert, I. M. Watson, E. Gu, Z. Chen, G. Zhang, and M. D. Dawson, Appl. Phys. Lett. **101**, 231110 (2012).
[9] G. Yamashita, E. Matsubara, M. Nagai, C. Kim, H. Akiyama, Y. Kanemitsu, and M. Ashida, Appl. Phys. Lett. **110**, 71108 (2017).
[10] W. Zhu, B. Mitchell, D. Timmerman, A. Uedono, A. Koizumi, and Y. Fujiwara, APL Mater. **4**, 056103 (2016).
[11] W. Zhu, R. Wei, D. Timmerman, T. Gregorkiewicz, B. Mitchell, Y. Fujiwara, and V. Dierolf, ACS Photonics **5**, 875 (2018).
[12] See Supplemental Material at http://link.aps.org/supplemental/10.1103/PhysRevB.101.245306 for the time profile of the terahertz pulse and the derivation for sheet mobility.
[13] W. Zhang, A. K. Azad, and D. Grischkowsky, Appl. Phys. Lett. **82**, 2841 (2003).
[14] B. G. Alberding, W. Robert Thurber, and E. J. Heilweil, J. Opt. Soc. Am. B **34**, 1392 (2017).
[15] F. Binet, J. Y. Duboz, J. Off, and F. Scholz, Phys. Rev. B **60**, 4715 (1999).
[16] A. Ajay, J. Schörmann, M. Jiménez-Rodriguez, C. B. Lim, F. Walther, M. Rohnke, I. Mouton, L. Amichi, C. Bougerol, M. I. Den Hertog, M. Eickhoff, and E. Monroy, J. Phys. D. Appl. Phys. **49**, 445301 (2016).
[17] J. Z. Zhang, J. Appl. Phys. **115**, 203704 (2014).
[18] N. Woodward, A. Nishikawa, Y. Fujiwara, and V. Dierolf, Opt. Mater. (Amsterdam, Neth.) **33**, 1050 (2011).
[19] I. S. Roqan, K. P. O'Donnell, R. W. Martin, P. R. Edwards, S. F. Song, A. Vantomme, K. Lorenz, E. Alves, and M. Bońkowski, Phys. Rev. B **81**, 085209 (2010).
[20] B. Mitchell, N. Hernandez, D. Lee, A. Koizumi, Y. Fujiwara, and V. Dierolf, Phys. Rev. B **96**, 064308 (2017).
[21] B. Mitchell, R. Wei, J. Takatsu, D. Timmerman, T. Gregorkiewicz, W. Zhu, S. Ichikawa, J. Tatebayashi, Y. Fujiwara, and V. Dierolf, ACS Photonics **6**, 1153 (2019).
[22] R. Wei, B. Mitchell, D. Timmerman, T. Gregorkiewicz, W. Zhu, J. Tatebayashi, S. Ichikawa, Y. Fujiwara, and V. Dierolf, Phys. Rev. B **100**, 081201(R) (2019).
[23] M. A. Reshchikov and H. Morkoç, J. Appl. Phys. **97**, 061301 (2005).
[24] M. A. Reshchikov, J. D. McNamara, H. Helava, A. Usikov, and Y. Makarov, Sci. Rep. **8**, 8091 (2018).
[25] K. Kanegae, M. Horita, T. Kimoto, and J. Suda, Appl. Phys. Express **11**, 071002 (2018).
[26] E. Kioupakis, Q. Yan, D. Steiauf, and C. G. Van De Walle, New J. Phys. **15**, 125006 (2013).
[27] S. F. Chichibu, A. Uedono, T. Onuma, T. Sota, B. A. Haskell, S. P. Denbaars, J. S. Speck, and S. Nakamura, Appl. Phys. Lett. **86**, 021914 (2005).
[28] W. Shockley and W. T. Read, Phys. Rev. **87**, 835 (1952).
[29] Y. Fujiwara, S. Takemoto, K. Nakamura, K. Shimada, M. Suzuki, K. Hidaka, Y. Terai, and M. Tonouchi, Physica B **401-402**, 234 (2007).